Applied Physics Letters ARTICLE scitation.org/journal/apl

Thermal stability of epitaxial α-Ga_2O_3 and $(Al,Ga)_2O_3$ layers on m-plane sapphire

Cite as: Appl. Phys. Lett. **119**, 062102 (2021); doi: 10.1063/5.0064278
Submitted: 21 July 2021 · Accepted: 23 July 2021 ·
Published Online: 9 August 2021

View Online

Export Citation

CrossMark

J. P. McCandless,[1,a)] C. S. Chang,[2,b)] K. Nomoto,[1] J. Casamento,[3] V. Protasenko,[1] P. Vogt,[3] D. Rowe,[3] K. Gann,[3] S. T. Ho,[3] W. Li,[1] R. Jinno,[1] Y. Cho,[1] A. J. Green,[4] K. D. Chabak,[4] D. G. Schlom,[3,5,6] M. O. Thompson,[3] D. A. Muller,[2,5] H. G. Xing,[1,3,5] and D. Jena[1,3,5]

AFFILIATIONS

[1]School of Electrical and Computer Engineering, Cornell University, Ithaca, New York 14853, USA
[2]School of Applied and Engineering Physics, Cornell University, Ithaca, New York 14853, USA
[3]Department of Material Science and Engineering, Cornell University, Ithaca, New York 14853, USA
[4]Air Force Research Laboratory, Sensors Directorate, Wright-Patterson AFB, Ohio 45433, USA
[5]Kavli Institute at Cornell for Nanoscale Science, Cornell University, Ithaca, New York 14853, USA
[6]Leibniz-Institut für Kristallzüchtung, Max-Born-Str. 2, Berlin 12489, Germany

[a)]**Author to whom correspondence should be addressed:** jpm432@cornell.edu
[b)]**Current Affiliation:** Research Laboratory of Electronics, Massachusetts Institute of Technology, Cambridge, MA 02139, USA.

ABSTRACT

Here, we have explored the thermal stability of α-$(Al,Ga)_2O_3$ grown by the molecular-beam epitaxy on m-plane sapphire under high-temperature annealing conditions for various Al compositions (i.e., 0%, 46%, and 100%). Though uncapped α-Ga_2O_3 undergoes a structural phase transition to the thermodynamically stable β-phase at high temperatures, we find that an aluminum oxide cap grown by atomic layer deposition preserves the α-phase. Unlike uncapped α-Ga_2O_3, uncapped α-$(Al,Ga)_2O_3$ at 46% and 100% Al content remain stable at high temperatures. We quantify the evolution of the structural properties of α-Ga_2O_3, α-$(Al,Ga)_2O_3$, and α-Al_2O_3 and the energy bandgap of α-Ga_2O_3 up to 900 °C. Throughout the anneals, the α-Ga_2O_3 capped with aluminum oxide retains its high crystal quality, with no substantial roughening.

Published under an exclusive license by AIP Publishing. https://doi.org/10.1063/5.0064278

Monoclinic β-Ga_2O_3 has garnered tremendous interest due to n-type doping control, large-area native substrates, a large energy bandgap of $E_g \sim 4.7$ eV, and breakdown electric fields reported to be as high as 5.3 MV/cm.[1–4] Because of the lattice mismatch and thermodynamic stability, it becomes increasingly difficult to increase the bandgap in β-$(Al,Ga)_2O_3$ through alloying with Al. At high Al% the β-$(Al,Ga)_2O_3$ phase becomes structurally unstable.[5–9]

In contrast, α-$(Al,Ga)_2O_3$ is isostructural with the trigonal sapphire crystal structure. Therefore, the stability of this phase increases with the increasing Al% since the lattice mismatch is reduced, eliminating the limits of the β-phase. Additionally, high-Al content films have a native substrate, sapphire, analogous to that of low-Al content β-phase films on β-Ga_2O_3 bulk substrates. The investigations of α-$(Al_xGa_{1-x})_2O_3$ have been performed by mist-chemical vapor deposition (CVD),[10–12] by MBE,[13,14] and by pulsed laser deposition (PLD).[15] High-quality α-$(Al_xGa_{1-x})_2O_3$ growth was recently achieved by MBE on m-plane sapphire with Al ranging from $x = 0 \rightarrow 1$. The energy bandgaps achieved are up to 8.6 eV, surpassing that of AlN and diamond.[14]

To take advantage of the large energy bandgaps, the electronic conductivity of α-$(Al,Ga)_2O_3$ must be controlled. α-Ga_2O_3 grown by mist-CVD has been successfully doped during growth with Sn and with Si.[16–19] With Sn doping, mobile electron densities of $n \sim 10^{17} - 10^{19}/cm^3$ were achieved, with the highest reported electron mobility of 65 cm^2/V s at $n \sim 1.2 \times 10^{18}/cm^3$ at room temperature.[20] For Si doping $n \sim 10^{18} - 10^{19}/cm^3$ was achieved with a room temperature mobility of $\mu_n \sim 32$ cm^2/V s for $n \sim 3 \times 10^{18}/cm^3$.[18]

Another doping approach—ion implantation—is attractive for ultra-wide bandgap layers since it offers conductivity control in the lateral directions, which is difficult in epitaxy. For example, it can be used to dope a transistor channel with low carrier concentrations for efficient gate modulation, and contact regions with high carrier concentrations for low-resistance contacts, without the need of regrowth. Typically implanted dopants require the high-temperature annealing

Published under an exclusive license by AIP Publishing

to electronically activate the carriers. For example, Sasaki *et al.* found that achieving above 60% activation in Si-implanted β-Ga_2O_3 required activation anneals up to 1000 °C.[21] Additionally, other processes for electronic devices (such as metallization) often employ high temperature anneals. For such steps, α-$(Al,Ga)_2O_3$ must retain its structural stability at the required high temperatures.

The stability of α-Ga_2O_3 under high-temperature anneals has been studied for films deposited on c-plane sapphire by atomic layer deposition (ALD) and mist-CVD.[14,22–25] Jinno *et al.* recently reported that mist-CVD grown α-Ga_2O_3 remains stable up to 660 °C and that the stability is thickness dependent.[25] They observed that by alloying α-Ga_2O_3 with Al, the films can be stabilized up to 750 °C with 2.5% Al and up to 850 °C with 20% Al.[23] α-$(Al,Ga)_2O_3$ with more than 60% Al remained stable up to 1100 °C. No method, besides Al alloying, has been reported to prevent the phase transformations of the α-Ga_2O_3. Moreover, no studies have investigated the thermal stability of such films grown on m-plane sapphire, or of films grown by MBE.

MBE is a growth technique worth studying due to the ability to have atomically sharp interfaces, high crystal quality, and precise control over doping profiles. In this work, we perform a systematic study of the structural stability of α-Ga_2O_3, α-$(Al,Ga)_2O_3$, and α-Al_2O_3 grown on m-plane sapphire by MBE under high-temperature anneals. Moreover, we identify that by using a protective capping layer (which we also refer to as an annealing mask), the α-Ga_2O_3 can be preserved under high-temperature anneals. α-$(Al,Ga)_2O_3$ and α-Al_2O_3 are structurally stable and do not need capping.

All the films discussed in this work were grown on m-plane sapphire substrates in a Veeco GEN 930 MBE system. The substrates were cleaved into $\sim 1 \times 1$ cm^2 squares, cleaned by a standard solvent procedure, and were indium mounted on 3 in. Si wafers. Surface adsorbates were out-gassed *in situ* for 30 min. at 900 °C as measured by a thermocouple. The Ga and Al were delivered from the effusion cells. Active oxygen was provided from a RF-power plasma source. During growth, the plasma power was maintained at 250 W for all samples.

The growth conditions and sample thicknesses of the seven samples studied are described in Table I. The substrate temperature T_{sub} was monitored by a thermocouple located in the center of the sample heater. Two Ga_2O_3 control samples, G1 and G2, were grown for this study. These samples were grown under different conditions to investigate the effect of the linear growth regime and of the Ga_2O desorption limited O-rich growth regime (subsequently referred to as the desorption regime) on the structural stability. The work by Vogt *et al.* shows that the linear growth regime is achieved with excess O such that Ga incorporates fully into the film. This results in a growth rate that (a) increases linearly with the supplied Ga flux and (b) is independent of the growth temperature.[26,27] The desorption regime is reached when T_{sub} is increased sufficiently for a fixed Ga flux, or when the Ga flux is increased sufficiently for a given T_{sub}. In the desorption regime, the growth rate is mediated by the competition between the Ga_2O_3 formation and the desorption of the volatile sub-oxide Ga_2O.

Three additional Ga_2O_3 samples M1, M2, and M3, were grown to investigate the effect of different anneal masks, Al_2O_3 (referred to as AlO_x), SiO_2, and Mo, respectively, (see Table I). An $(Al,Ga)_2O_3$ sample (sample A1) was grown with 46% Al as determined by x-ray diffraction (XRD). The last sample investigated was homoepitaxial Al_2O_3 (sample A2). Additionally, sample A2 had a 4 nm $(Al_{0.75}, Ga_{0.25})_2O_3$ layer grown before the Al_2O_3. This 4 nm layer creates an interface from which x-ray interference will occur, generating a diffraction pattern. Without this layer, the XRD measurements would not differentiate between the homoepitaxial film and the much thicker substrate.

Figure 1 shows the experimental procedure devised for studying the phase stability at high temperature. After growth, XRD measurements were used first to identify the crystalline phase. 2θ-ω scans were performed, aligning to the $30\bar{3}0$ sapphire substrate peak. These out-of-plane scans measure the Bragg planes parallel to the aligned substrate peak. From these scans, the existence of other crystal phases (e.g., β-phase) aligned to the $(10\bar{1}0)$ sapphire is determined based on the peak locations. Rocking curve measurements were also obtained with the x-ray detector fixed at a given Bragg angle. Atomic force microscopy (AFM) was performed for all samples for direct measurement of the surface morphology. Optical transmission spectroscopy measurements in the ultraviolet and visible (UV-VIS) part of the spectrum were performed as a function of the photon energy to monitor the energy bandgap shifts that result from the structural phase transformations of the crystal.

Anneal masks were deposited on samples M1, M2, and M3 as described in Table I. The mask thickness was determined by profilometry measurements of a shadow-masked Si chip which was deposited concurrently with the sample. The unmasked control samples (G1 and G2), the masked samples (M1, M2, and M3), and the unmasked Al containing samples (A1 and A2) were annealed

TABLE I. Description of the MBE-grown α-$(Al,Ga)_2O_3$/m-plane sapphire samples studied in this work.

				Flux (atoms/nm^2 s)				Anneal mask		
Sample	Grown structure	Growth regime	Growth temp. (°C)	Ga	Al	O_2 flow (sccm)	Film thickness (nm)	Material	Deposition Technique	Thickness (nm)
G1	Ga_2O_3	Linear	680	0.63	⋯	1.40	58	⋯	⋯	⋯
G2	Ga_2O_3	Desorption	750	1.34	⋯	1.40	65	⋯	⋯	⋯
M1	Ga_2O_3	Linear	660	0.63	⋯	1.40	57	Al_2O_3	ALD	29.5
M2	Ga_2O_3	Linear	720	0.63	⋯	1.40	59	SiO_2	PECVD	48.2
M3	Ga_2O_3	Desorption	770	0.86	⋯	1.40	65	Mo	Sputtering	>115
A1	$(Al,Ga)_2O_3$	⋯	625	0.23	0.21	0.67	117	⋯	⋯	⋯
A2	Al_2O_3	⋯	680	⋯	0.45	0.67	48	⋯	⋯	⋯

Published under an exclusive license by AIP Publishing

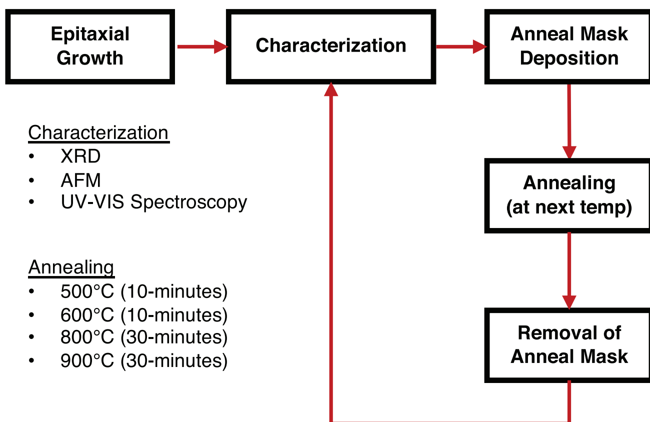

FIG. 1. The process flow to investigate high-temperature stability is shown. All samples were annealed concurrently at increasing temperatures in a rapid thermal annealer in the presence of N_2 flow.

simultaneously in a rapid thermal anneal (RTA) system in a N_2 environment.

After the anneal, the SiO_2 and AlO_x masks were etched with HF (49%), and the Mo was etched with $HF{:}HNO_3$ (1:1). The samples were characterized, the anneal masks were re-deposited (for M1, M2, and M3), and the samples were annealed at the next temperature.

The criteria for evaluating the stability of a given sample were based on the continued presence of the sharp and intense α-phase diffraction peak, the lack of appearance of additional XRD peaks, and the stability of the energy bandgap of the epitaxial layers after annealing. The structural quality was tracked with the full-width at half-max (FWHM) value of the XRD rocking curve and the AFM surface roughness. Finally, after the 900 °C anneal, scanning transmission electron microscopy (STEM) using aberration-corrected Titan Themis was performed on samples G1 and on M1 at a beam voltage of 300 keV. This allowed for direct imaging and determination of crystal phase, crystal quality, interfacial quality, and defect-types resulting from the high-temperature annealing. Cross-sectional TEM specimens were prepared using a Thermo Fisher Helios G4 UX focused ion beam (FIB) with 5 keV as the final milling voltage to reduce the damage. Carbon and platinum layers were deposited on the sample surface prior to FIB to minimize the ion beam damage.

Figure 2 shows the evolution of the 2θ-ω XRD spectra as a function of annealing temperature of (a) the Ga_2O_3 control sample G1, (b) the sample masked with AlO_x M1, (c) the $(Al,Ga)_2O_3$ sample A1, and (d) the epitaxial Al_2O_3 sample A2. The rocking curve data are summarized in the supplementary section. Sample G1, the uncapped sample grown in the linear, full Ga incorporation regime, remained α-phase through an annealing temperature of 600 °C, as indicated by the presence of the $30\bar{3}0$ peak in Fig. 2(a). After the 800 °C anneal, it converted to the thermodynamically stable β-phase as indicated by the presence of the β-Ga_2O_3 020 diffraction peak. This behavior was also observed for uncapped sample G2, the sample grown by MBE in the desorption regime (see supplementary material). This observation in uncapped MBE-grown α-Ga_2O_3 epitaxial layers on m-plane sapphire is in agreement with the report of mist-CVD deposited α-Ga_2O_3 on c-plane sapphire. The uncapped α-phase Ga_2O_3 epitaxial layers convert to the

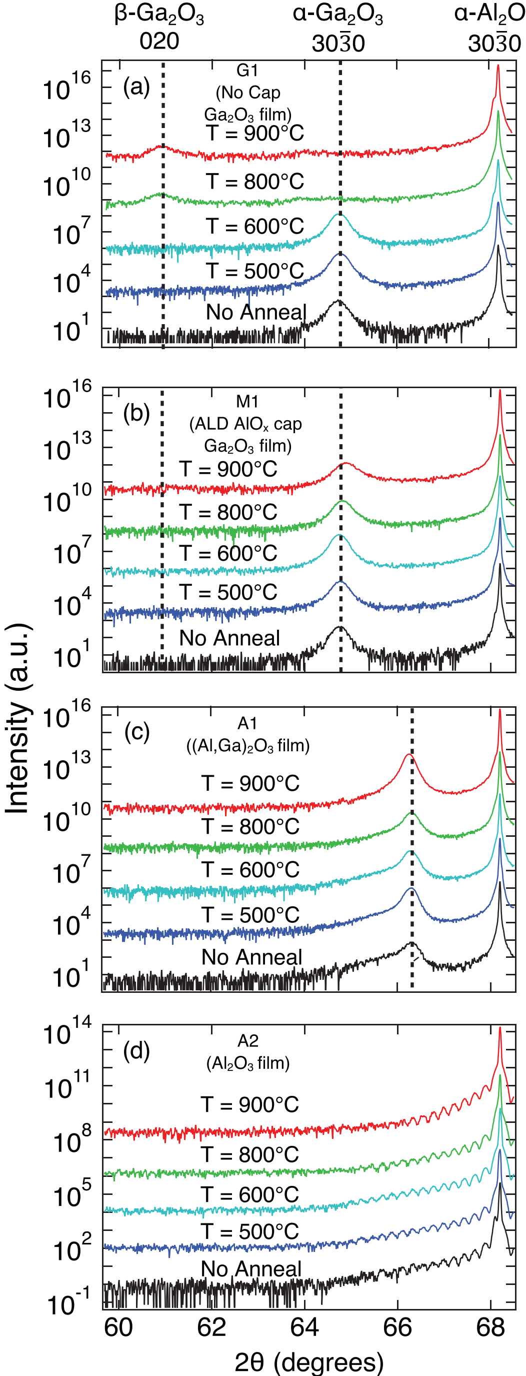

FIG. 2. The XRD measurements are shown for (a) the uncapped Ga_2O_3 control sample grown in the linear growth regime (G1), (b) the AlO_x-capped sample (M1), (c) the $(Al,Ga)_2O_3$ sample (A1), and (d) the Al_2O_3 sample (A2).

β-phase beyond ~600 °C anneal by both growth methods, and on both orientations of the sapphire substrate.[25]

On the other hand, the ALD aluminum oxide-capped α-Ga_2O_3 sample M1, the uncapped $(Al,Ga)_2O_3$ sample A1, and uncapped

Published under an exclusive license by AIP Publishing

Al_2O_3 sample A2 remained stable in the α-phase throughout the high-temperature annealing study. This is indicated by the stability of the $30\bar{3}0$ diffraction peak of samples M1 and A1, and the fact that no additional peaks appear. The crystal quality of sample M1 was further quantified by a rocking curve measurement of the Ga_2O_3 $30\bar{3}0$ diffraction peak. The rocking curve FWHM of the sample decreased from 0.59° to 0.41° after the final anneal. The 2θ diffraction peak of sample M1 broadened and shifted to a higher angle by approximately 0.07° after the 900 °C anneal as seen in Fig. 2 (b). The shift is due to some Al diffusion from the mask into the surface of the film after the 900 °C anneal. Secondary ion mass spectrometry and reciprocal space maps were performed and indicate ~3.5% Al with an exponentially decaying profile within the first ~24 nm of the Ga_2O_3 film. This is discussed in the supplementary material.

After the 900 °C anneal of sample A1, there is a downward shift in the 2θ value of the $30\bar{3}0$ peak by approximately 0.05° [Fig. 2 (c)]. During the x-ray diffraction measurements, the azimuth of the substrate was not controlled. This shift is likely due to the anisotropy of the crystal. In contrast, the XRD peak spectra of sample A2 remained unaffected through the annealing study [Fig. 2 (d)].

The SiO_2-capped α-Ga_2O_3 sample M2 remained in the α-phase through the 800 °C anneal. Nevertheless, after the 900 °C anneal, the α-Ga_2O_3 peak disappeared (and no β-phase peak appeared), indicating the sample had become amorphous. This behavior was also observed with the Mo-capped sample, M3. One hypothesis for the amorphization of samples M2 and M3 is that a reaction between the mask (SiO_2 and Mo, respectively) and the Ga_2O_3 film occurred during the high-temperature anneal. The resulting silicide and MoO_x compound crystallized, affecting the energy landscape of the crystal. This resulted in the loss of the metastable α-phase when cooled. More work is needed to investigate and confirm this hypothesis. It is possible that Mo and SiO_2 caps may stabilize the α-phase if deposited under different conditions (e.g., deposition technique, thickness, etc.) than used. The XRD data and additional discussion are provided in the supplementary material.

The evolution of the energy bandgap follows that of the XRD peaks with high-temperature annealing, as determined by absorption spectroscopy in the UV-VIS regime. The product squared (direct bandgap) of the absorption coefficient and photon energy vs the photon energy (Tauc plot) are plotted in Figs. 3(a)–3(c) for samples G1, M1, and M2. Note that all samples were calculated assuming a direct bandgap to emphasize that a shift in the bandgap occurred, not an artificial shift from assuming an indirect bandgap. The Al-containing films (A1 and A2) are not shown, for the bandgap exceeds the available photon energy of the equipment. The extracted energy bandgaps are then plotted as a function of the annealing temperature for samples G1, M1, and M2 in Figs. 3(d)–3(f).

All α-Ga_2O_3 samples had an energy bandgap of ~5.3 eV when measured after MBE growth (before annealing). After the 800 °C anneal, sample G1 showed a clear reduction in the bandgap in the absorption curve to 5.0 eV. This corroborates the indication from XRD that the sample underwent a structural transformation from the α-phase to the β-phase. The energy bandgap of the ALD AlO_x-capped sample M1 remained stable throughout all of the anneals. The SiO_2-capped α-Ga_2O_3 sample M2 remained stable up to 800 °C anneal, in agreement with what was observed by XRD. After the 900 °C anneal, there was a downward shift in the bandgap to 5.0 eV coincident with the disappearance of the α-phase $30\bar{3}0$ XRD peak. Amorphous Ga_2O_3 was sputtered onto a m-sapphire substrate, and the absorption spectrum was measured (the results are shown with a dashed line). The spectrum of sample M2 after the 900 °C anneal and the structural transition show an absorption spectrum that is similar to the amorphous Ga_2O_3 sample.

AFM images of the surface of each sample were acquired after each annealing step. The smoothness of the surface is an important factor in the use of these epitaxial layers in electronic devices. In Fig. 4, $2 \times 2\,\mu m^2$ scans for the samples after growth and after the 900 °C anneal are shown, and the rms roughness of the samples after each anneal step is plotted in Fig. 5. It is worth noting that the AlO_x cap crystallized after the 900 °C anneal and, therefore, was not removed during the wet etch. Thus, the rms roughness (R_q) and AFM scan correspond to the mask. Similarly, the Mo cap underwent a chemical reaction which formed MoO_x, which was not removed by the wet etch (this is discussed in more detail in the supplementary material).

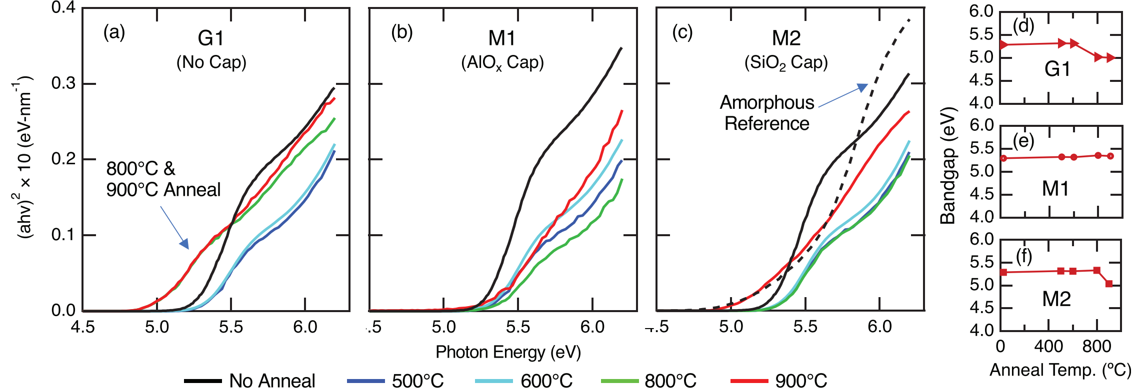

FIG. 3. Tauc plots are shown for (a) the uncapped Ga_2O_3 control sample (G1), (b) the AlO_x-capped sample (M1), and (c) the SiO_2-capped sample (M2). After the higher-temperature anneals, G1 and M2 show a decrease in the bandgap associated with the evolution to the β-phase and to the amorphous state, respectively. In contrast, M1 remains stable through the anneals. (d)–(f) Show the bandgap energies obtained from the Tauc plots as a function of the anneal temperature for (d) the Ga_2O_3 control sample, (e) the AlO_x-capped sample, and (f) the SiO_2-capped samples.

Published under an exclusive license by AIP Publishing

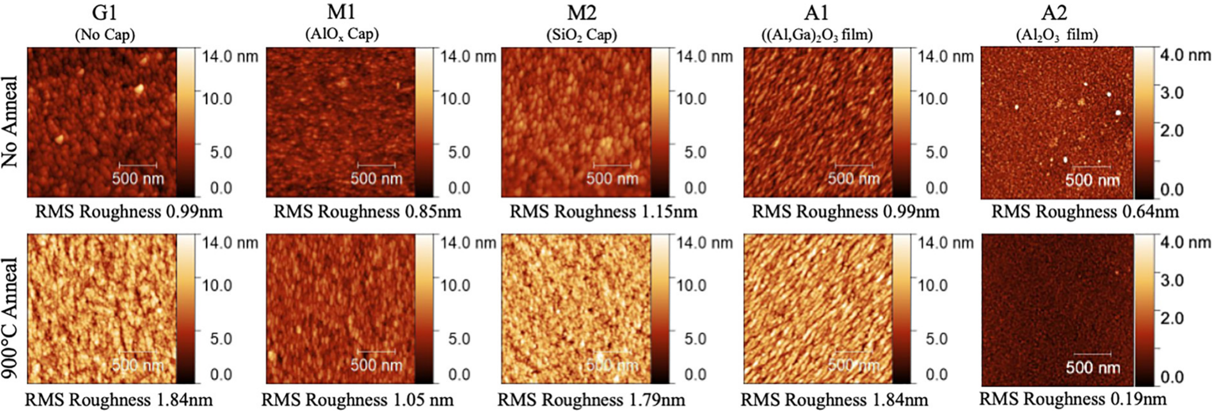

FIG. 4. The $2 \times 2\ \mu m^2$ AFM scans and the rms roughnesses are shown for two cases—(i) after growth and (ii) after the 900 °C anneal for the non-masked, control sample (G1), the AlO_x and SiO_2-capped samples (M1 and M2, respectively), for the Al alloyed film (A1), and for the Al_2O_3 film (A2).

The uncapped, control sample G1 is shown in Fig. 5 (a). The capped samples are shown in Fig. 5 (b), and the Al containing samples are shown in Fig. 5 (c). The uncapped control samples G1 and G2 (not shown), along with the Mo-capped sample M3 displayed a (monotonically) increasing roughness with each annealing step. The SiO_2-capped sample experienced an increase in roughness after growth with annealing and then a slight decrease in roughness with the 800 °C and 900 °C anneals. This resulted in the film being rougher than it was before annealing. In contrast, the sample masked with AlO_x retained a fairly steady surface morphology going from an rms roughness of 0.85 to 1.05 nm; the variation observed may be due to some variation in the measurement location. Sample A1 showed some roughening during the annealing steps as its rms roughness went from 0.99 to 1.84 nm, while sample A2 actually became smoother with annealing, decreasing from an rms roughness of 0.64 to 0.19 nm. In summary, the non-capped, control samples became rougher with anneal, a trend which continued through the α-Ga_2O_3 phase change. The only capped sample to remain smooth was the AlO_x-capped sample; the Al_2O_3 homoepitaxial grown film also became smoother.

STEM images were taken of the capped α-Ga_2O_3 sample M1 and the uncapped control sample G1, along with another as-grown (unannealed) sample for reference. Figure 6 (a) shows the STEM image of the MBE-grown unannealed α-Ga_2O_3 control sample. The interface with the m-plane sapphire is sharp. The images are taken along the [0001] azimuth of the sapphire substrate. The out-of-plane growth direction is $[10\bar{1}0]$. Figures 6 (b)–6(d) are of the control sample G1

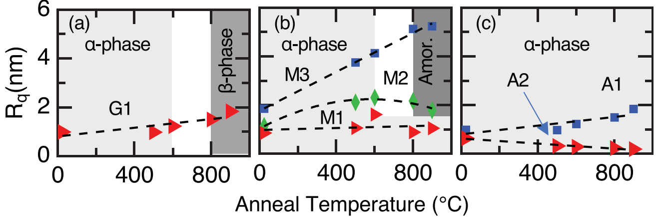

FIG. 5. The rms roughness obtained from $2 \times 2\ \mu m^2$ scans after each anneal step. The uncapped Ga_2O_3 control sample, G1, is shown in (a), the capped Ga_2O_3 samples are shown in (b), and the Al containing samples are shown in (c).

after it was annealed at 900 °C. A ~7 nm amorphous layer is observed at the surface of the uncapped sample after the 900 °C anneal as seen in Figs. 6(b) and 6(c). More importantly, the STEM images provide a direct confirmation that the uncapped Ga_2O_3 indeed converted from the α-phase to the β-phase, as was concluded from the XRD and energy bandgap measurements discussed earlier. The β-phase stabilized in a manner such that the image is along the $[1\bar{1}\bar{2}]$ azimuth, which is therefore parallel to the [0001] direction of the corundum phase m-plane sapphire substrate, see Fig. 6 (d). Figures 6 (e)–(g) are of the ALD AlO_x-capped α-Ga_2O_3 sample M1 after the 900 °C anneal. As seen in Fig. 6(g), the Ga_2O_3 remained α-phase after the anneal. The capping layer of M1 crystallized after the 900 °C anneal as shown in Fig. 6 (f). The interface between the cap layer and the α-Ga_2O_3 is rough for the conditions used here. Whether it improves by limiting the number of anneals, etches, and re-depositions experienced by the sample would be of interest in future studies.

There are at least three factors which enable the AlO_x mask to stabilize the α-phase, though the extent of each needs additional study. (1) Up to 800 °C, before the Al diffusion and before the crystallization of the mask, the AlO_x mask suppresses the decomposition of the film or potential loss of O. (2) After 900 °C, there is some Al diffusion which can promote phase stability. (3) The AlO_x mask crystallizes, which applies strain to the α-Ga_2O_3 and can aid in phase stabilization.

Table II summarizes the energy bandgaps (E_g), rocking curve FWHM, and rms roughnesses (R_q) for all the samples as-grown and after the 900 °C anneal. For the cases when the film became amorphous or when the film converted to the β-phase, the rocking curves were not measured.

Based on the cumulative evidence from XRD, spectroscopy, AFM, and TEM, sample M1 was the only α-Ga_2O_3 sample that retained the α-phase at prolonged 900 °C annealing. Thus, we conclude that by masking a sample with ALD AlO_x, undoped MBE-grown α-Ga_2O_3 on m-plane sapphire can be stabilized up to 900 °C annealing temperatures with no significant roughening and improvement in the crystal quality based on rocking curve measurements. Further, the crystallization of the ALD aluminum oxide cap layer was observed, which could enable certain forms of heterostructures based on the electronic properties of this layer. We observed that uncapped

Published under an exclusive license by AIP Publishing

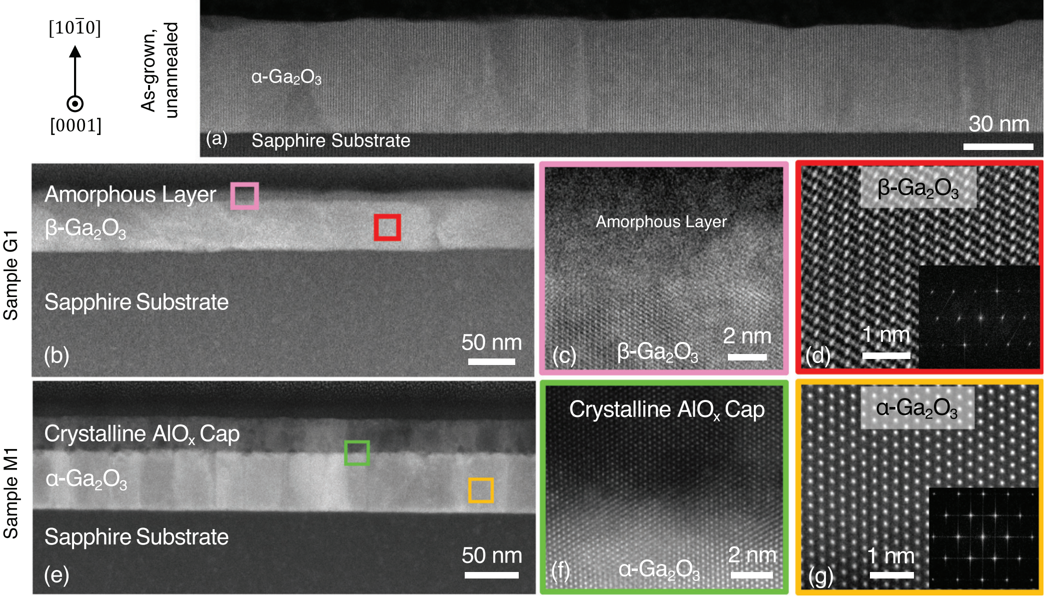

FIG. 6. Confirmation of the Ga_2O_3 phases by STEM. (a) shows an as-grown, unannealed α-Ga_2O_3 sample. (b)–(d) are of sample G1, the uncapped Ga_2O_3 control sample which converted from the α-phase to the β-phase after annealing. (c) shows a thin amorphous layer created on the top surface of β-Ga_2O_3. (d) shows the atomic structure of the β-Ga_2O_3 imaged along the $[11\bar{2}]$ azimuth and the corresponding diffraction pattern of the lattice. (e)–(g) are of the AlO_x-capped sample M1, which remained α-phase after the 900 °C anneal. (f) shows the interface of the epitaxial α-Ga_2O_3 with the crystallized AlO_x cap. (g) shows α-Ga_2O_3 structure with a diffractogram showing a hexagonal reciprocal lattice as an inset.

MBE-grown α-Ga_2O_3 films grown on m-plane sapphire were stable up to 600 °C anneal and then converted to the β-phase after annealing at 800 °C, similar to what is observed for mist-CVD growths on c-plane sapphire. We also observed that α-Ga_2O_3 samples capped with SiO_2 or Mo become amorphous after 800 °C anneals. Finally, we have shown that the films with Al content above 46% remain stable through 900 °C anneal even without a cap layer; the roughness of the α-Al_2O_3 epitaxial films reduced upon annealing. This work provides a pathway for doping studies by ion implantation by identifying the conditions for preserving the crystalline phase of α-$(Al,Ga)_2O_3$ epitaxial layers grown by MBE on m-plane sapphire wafers spanning energy bandgaps from 5.3 to 8.6 eV.

TABLE II. The rocking curve FWHM, bandgap, and rms roughness are listed for samples as-grown and after the 900 °C anneal.

Sample	Mask	Phase post 900 °C anneal	Rocking curve FWHM (deg)	E_g (eV)	R_q (nm)
G1	Uncapped	β	0.67	5.3	0.99
			⋯	5.0	1.84
G2	Uncapped	β	0.55	5.3	1.10
			⋯	5.0	1.59
M1	Al_2O_3	α	0.59	5.3	0.85
			0.41	5.3	1.05
M2	SiO_2	Amorphous	0.53	5.3	1.15
			⋯	5.0	1.79
M3	Mo	Amorphous	0.55	5.3	1.86
			⋯	5.0	5.24
A1	⋯	α	0.28	⋯	0.99
			0.24	⋯	1.84
A2	⋯	α	⋯	⋯	0.64
			⋯	⋯	0.19

See the supplementary material for all AFM images, rocking curve values, RSM data, SIMS data, and XPS data. Additional XRD and absorption data not shown in the main text are also included.

The authors would like to thank Shin Mou, Tadj Asel, and Adam Neal of the Air Force Research Laboratory for their helpful discussions and feedback related to this effort. This research was supported by the Air Force Research Laboratory-Cornell Center for Epitaxial Solutions (ACCESS) under Grant No. FA9550-18-1-0529. J.P.M. acknowledges the support of a National Science Foundation Graduate Research Fellowship under Grant No. DGE-1650441. This work used the CCMR and CESI Shared Facilities partly sponsored by the NSF MRSEC program (No. DMR-1719875) and MRI (No. DMR-1338010), the National Science Foundation Platform for the Accelerated Realization, Analysis, and Discovery of Interface Materials (PARADIM) under Cooperative Agreement No. DMR-1539918, and the Kavli Institute at Cornell (KIC).

DATA AVAILABILITY

The data that support the findings of this study are available from the corresponding author upon reasonable request.

Published under an exclusive license by AIP Publishing

REFERENCES

[1]A. J. Green, K. D. Chabak, E. R. Heller, R. C. Fitch, M. Baldini, A. Fiedler, K. Irmscher, G. Wagner, Z. Galazka, S. E. Tetlak, A. Crespo, K. Leedy, and G. H. Jessen, "3.8-MV/cm Breakdown strength of MOVPE-grown Sn-doped β-Ga_2O_3 MOSFETs," IEEE Electron Device Lett. **37**, 902–905 (2016).

[2]Z. Xia, H. Chandrasekar, W. Moore, C. Wang, A. J. Lee, J. McGlone, N. K. Kalarickal, A. Arehart, S. Ringel, F. Yang, and S. Rajan, "Metal/$BaTiO_3$/β-Ga_2O_3 dielectric heterojunction diode with 5.7 MV/cm breakdown field," Appl. Phys. Lett. **115**, 252104 (2019).

[3]K. D. Chabak, N. Moser, A. J. Green, D. E. Walker, S. E. Tetlak, E. Heller, A. Crespo, R. Fitch, J. P. McCandless, K. Leedy, M. Baldini, G. Wagner, Z. Galazka, X. Li, and G. Jessen, "Enhancement-mode Ga_2O_3 wrap-gate fin field-effect transistors on native (100) β-Ga_2O_3 substrate with high breakdown voltage," Appl. Phys. Lett. **109**, 213501 (2016).

[4]C. Joishi, S. Rafique, Z. Xia, L. Han, S. Krishnamoorthy, Y. Zhang, S. Lodha, H. Zhao, and S. Rajan, "Low-pressure CVD-grown β-Ga_2O_3 bevel-field- plated Schottky barrier diodes," Appl. Phys. Express **11**, 031101 (2018).

[5]A. F. U. Bhuiyan, Z. Feng, J. M. Johnson, H. L. Huang, J. Sarker, M. Zhu, M. R. Karim, B. Mazumder, J. Hwang, and H. Zhao, "Phase transformation in MOCVD growth of $(Al_xGa_{1-x})_2O_3$ thin films," APL Mater. **8**, 031104 (2020).

[6]F. Zhang, K. Saito, T. Tanaka, M. Nishio, M. Arita, and Q. Guo, "Wide bandgap engineering of $(AlGa)_2O_3$ films," Appl. Phys. Lett. **105**, 162107 (2014).

[7]T. Oshima, T. Okuno, N. Arai, Y. Kobayashi, and S. Fujita, "β-$Al_{2x}Ga_{2-2x}O_3$ thin film growth by molecular beam epitaxy," Jpn. J. Appl. Phys., Part 1 **48**, 070202 (2009).

[8]S. Mu, M. Wang, H. Peelaers, C. G. Van, and D. Walle, "First-principles surface energies for monoclinic Ga_2O_3 and Al_2O_3 and consequences for cracking of $(Al_xGa_{1-x})_2O_3$," APL Mater. **8**, 091105 (2020).

[9]V. G. Hill, R. Roy, and E. Osborn, "The system alumina-gallia-water," J. Am. Ceram. Soc. **35**, 135–142 (1952).

[10]G. T. Dang, T. Yasuoka, Y. Tagashira, T. Tadokoro, W. Theiss, and T. Kawaharamura, "Bandgap engineering of α-$(Al_xGa_{1-x})_2O_3$ by a mist chemical vapor deposition two-chamber system and verification of Vegard's law," Appl. Phys. Lett. **113**, 062102 (2018).

[11]T. Uchida, R. Jinno, S. Takemoto, K. Kaneko, and S. Fujita, "Evaluation of band alignment of α-Ga_2O_3/α-$(Al_xGa_{1x})_2O_3$ heterostructures by x-ray photoelectron spectroscopy," Jpn. J. Appl. Phys., Part 1 **57**, 040314 (2018).

[12]H. Ito, K. Kaneko, and S. Fujita, "Growth and band gap control of corundum-structured α-$(AlGa)_2O_2$ Thin films on sapphire by spray-assisted mist chemical vapor deposition," Jpn. J. Appl. Phys., Part 1 **51**, 100207 (2012).

[13]R. Kumaran, T. Tiedje, S. E. Webster, S. Penson, and W. Li, "Epitaxial Nd-doped α-$(Al_{1x}Ga_x)_2O_3$ films on sapphire for solid-state waveguide lasers," Opt. Lett. **35**, 3793 (2010).

[14]R. Jinno, C. S. Chang, T. Onuma, Y. Cho, S. T. Ho, D. Rowe, M. C. Cao, K. Lee, V. Protasenko, D. G. Schlom, D. A. Muller, H. G. Xing, and D. Jena, "Crystal orientation dictated epitaxy of ultrawide-bandgap 5.4-to 8.6-eV α-$(AlGa)_2O_3$ on m-plane sapphire," Sci. Adv. **7**, eabd5891 (2021).

[15]M. Lorenz, S. Hohenberger, E. Rose, and M. Grundmann, "Atomically stepped, pseudomorphic, corundum-phase $(Al_{1-x}Ga_x)_2O_3$ thin films ($0 \le x < 0.08$) grown on R-plane sapphire," Appl. Phys. Lett. **113**, 231902 (2018).

[16]T. Kawaharamura, G. T. Dang, and M. Furuta, "Successful growth of conductive highly crystalline Sn-doped α-Ga_2O_3 thin films by fine-channel mist chemical vapor deposition," Jpn. J. Appl. Phys., Part 1 **51**, 040207 (2012).

[17]K. Akaiwa and S. Fujita, "Electrical conductive corundum-structured α-Ga_2O_3 Thin films on sapphire with tin-doping grown by spray-assisted mist chemical vapor deposition," Jpn. J. Appl. Phys., Part 1 **51**, 070203 (2012).

[18]T. Uchida, K. Kaneko, and S. Fujita, "Electrical characterization of Si-doped n-type α-Ga_2O_3 on sapphire substrates," MRS Adv. **3**, 171–177 (2018).

[19]K. Akaiwa, K. Kaneko, K. Ichino, and S. Fujita, "Conductivity control of Sn-doped α-Ga_2O_3 thin films grown on sapphire substrates," Jpn. J. Appl. Phys., Part 1 **55**, 1202BA (2016).

[20]K. Akaiwa, K. Ota, T. Sekiyama, T. Abe, T. Shinohe, and K. Ichino, "Electrical properties of Sn-doped α-Ga_2O_3 films on m-plane sapphire substrates grown by mist chemical vapor deposition," Phys. Status Solidi a **217**, 1900632 (2020).

[21]K. Sasaki, M. Higashiwaki, A. Kuramata, T. Masui, and S. Yamakoshi, "Si-Ion implantation doping in β-Ga_2O_3 and its application to fabrication of low-resistance ohmic contacts," Appl. Phys. Express **6**, 086502 (2013).

[22]S.-D. Lee, K. Akaiwa, and S. Fujita, "Thermal stability of single crystalline alpha gallium oxide films on sapphire substrates," Phys. Status Solidi c **10**, 1592–1595 (2013).

[23]S.-D. Lee, Y. Ito, K. Kaneko, and S. Fujita, "Enhanced thermal stability of alpha gallium oxide films supported by aluminum doping," Jpn. J. Appl. Phys., Part 1 **54**, 030301 (2015).

[24]J. Moloney, O. Tesh, M. Singh, J. W. Roberts, J. C. Jarman, L. C. Lee, T. Huq, J. Brister, S. Karboyan, M. Kuball, P. Chalker, R. Oliver, and F. C. Massabuau, "Atomic layer deposited α-Ga_2O_3 solar-blind photodetectors," J. Phys. D: Appl. Phys. **52**, 475101 (2019).

[25]R. Jinno, K. Kaneko, and S. Fujita, "Thermal stability of α-Ga_2O_3 films grown on c-plane sapphire substrates via mist-CVD," AIP Adv. **10**, 115013 (2020).

[26]P. Vogt and O. Bierwagen, "Reaction kinetics and growth window for plasma-assisted molecular beam epitaxy of Ga_2O_3: Incorporation of Ga vs. Ga_2O desorption," Appl. Phys. Lett. **108**, 072101 (2016).

[27]P. Vogt and O. Bierwagen, "Quantitative subcompound-mediated reaction model for the molecular beam epitaxy of III-VI and IV-VI thin films: Applied to Ga_2O_3, In_2O_3, and SnO2," Phys. Rev. Mater. **2**, 120401 (2018).

Published under an exclusive license by AIP Publishing

Thermal stability of epitaxial α-Ga_2O_3 and $(Al,Ga)_2O_3$ layers on m-plane sapphire

Supplemental Material

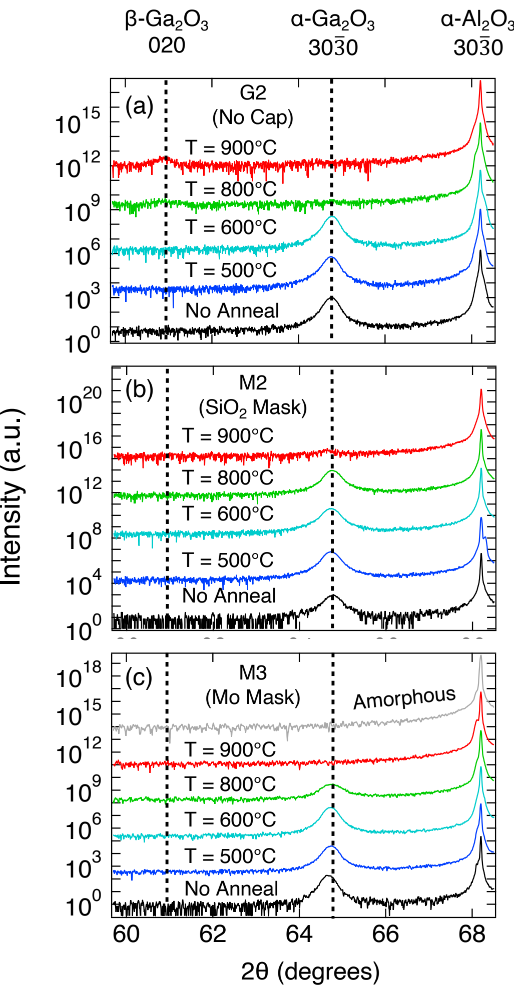

FIG. S1. The XRD 2θ-ω scans are shown for (a) the uncapped Ga_2O_3 control sample grown in the desorption growth regime (G2), (b) the SiO_2 capped sample (M2), and (c) the the Mo capped sample, M3

Figure S1 shows the 2θ-ω scans for the additional samples not shown in the main text (see Table I), Figs. S1(a) sample G2, (b) sample M2, and (c) sample M3, which correspond to the control sample grown in the desorption growth regime, the SiO_2-capped sample, and the Mo-capped sample, respectively. Sample G2 remained in the α-phase through the 600°C anneal, then converted to the β-phase during the 800°C anneal as evidenced by the diffraction peak at 60.94°. This is the same behavior as was observed for the control sample grown in the linear regime, sample G1. The sample capped with SiO_2, Fig. S1(b), remained stable through the 800°C. However, after the 900°C anneal there was no peak present indicating the sample had become amorphous. This behavior was also observed with the Mo capped sample shown in Fig. S1(c).

For comparison, 124 nm of amorphous Ga_2O_3 was sputtered on to a m-sapphire substrate. The XRD from this amorphous reference is shown in Fig. S1c. The sapphire substrate was mounted to a Si carrier wafer and an RF Magnetron sputtering system with an AJA Ga_2O_3 target at room temperature was used. The sputtering was done at 5 mTorr pressure, with an atmosphere of 9:1 (Ar:O_2) for 60 minutes with a 150 W power.

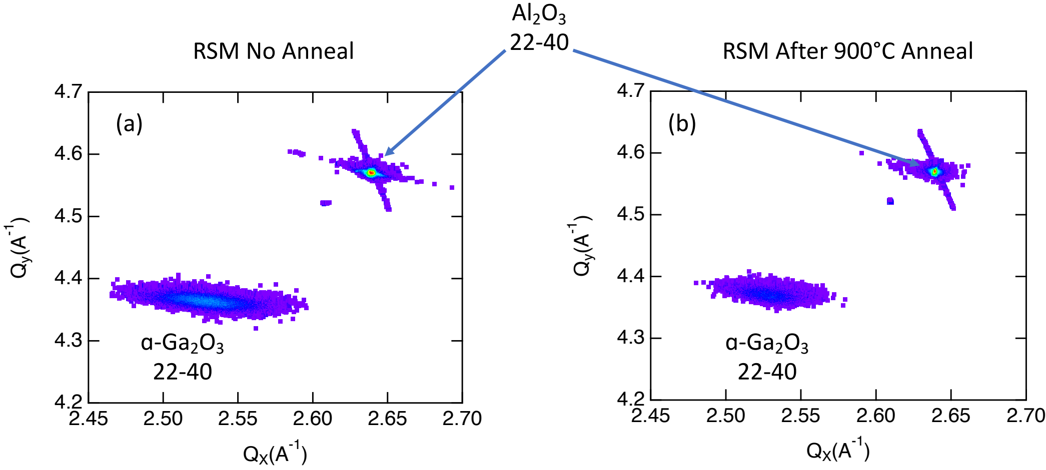

FIG. S2. A reciprocal space map for sample M1 (a) as-grown and (b) after the 900°C anneal.

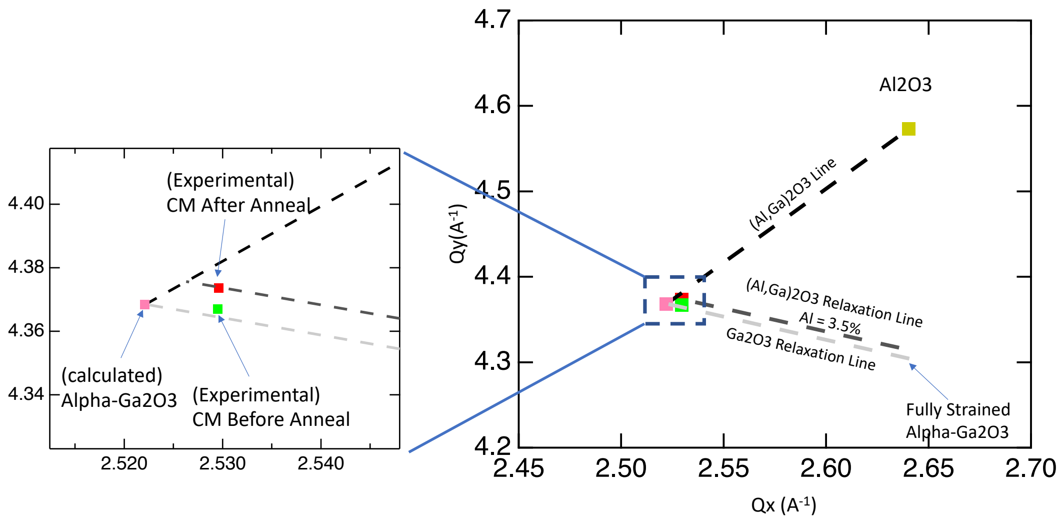

FIG. S3. Extracted peak positions from the reciprocal space map are shown. After the anneal, there is a clear upward shift in Qy.

Sample M1, the AlO_x capped sample, displayed an upward shift by 0.07°in the diffraction peak location after the 900°C anneal, as mentioned in the text. Fig. S2 plots an asymmetric reciprocal

space map (RSM) for Fig. S2(a) the as-grown sample and Fig. S2(b) after the 900°C anneal. For the measurements, the diffractometer is aligned to the Al_2O_3 $22\bar{4}0$ peak. A "center-of-mass" type calculation of the RSM intensities was used to determine the peak locations which are shown in Fig. S3. The $(Al, Ga)_2O_3$ line shows where the diffraction peak should be as the Al is increased, assuming no strain. Similarly, the diffraction peak moves along the relaxation line as the strain is increased.

Figure S3 shows a shift in Qy. This likely indicates there is some Al diffusion into the film (causing a shift up and to the right) accompanied by relaxation (a shift up and toward the left).

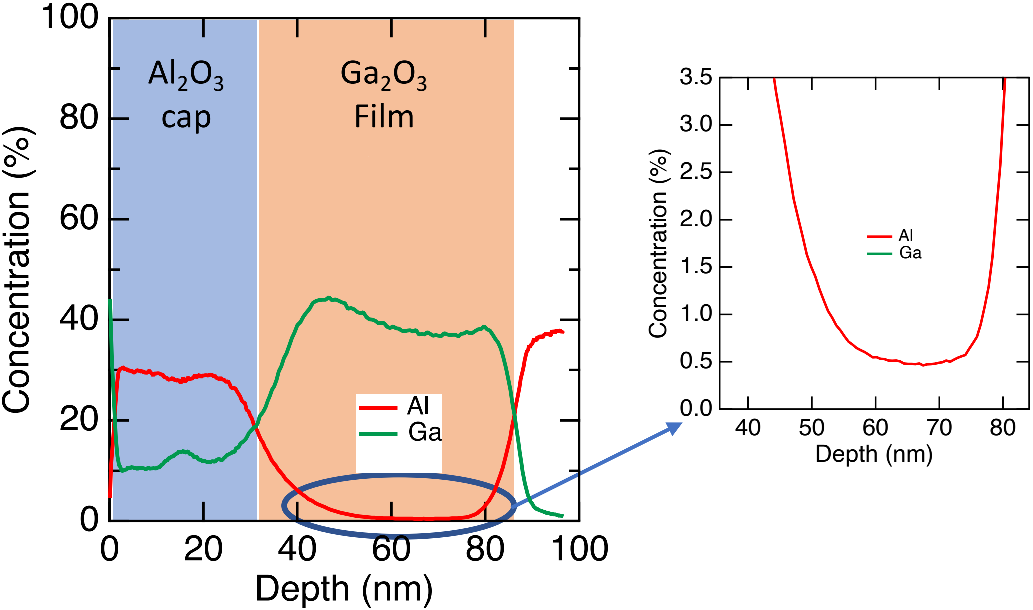

FIG. S4. Secondary ion mass spectroscopy (SIMS) was performed to quantify the Al and to better understand its distribution within the the film.

Next, secondary ion mass spectroscopy (SIMS) was performed to gain additional insight into the Al and Ga interdiffusion. The SIMS profile is shown in Fig. S4. It is clear that there is some Al and Ga interdiffusion in the cap and the surface of the epitaxial layer and at the film-substrate interface. A portion of the Al tail at the cap-film interface is driven in during the SIMS measurement. The Al diffusion from the substrate into the film we do not believe contributed to the stabilization of the film, for this diffusion would also occur in the control samples. From the cap, the Al profile decays with increasing depth – which is expected from thermal diffusion and from a SIMS tail. The Al tail is ~ 24 nm in length (from 31 nm to 55 nm). The Al profile then

flattens out at 0.5%. The average Al content from SIMS is 4%.

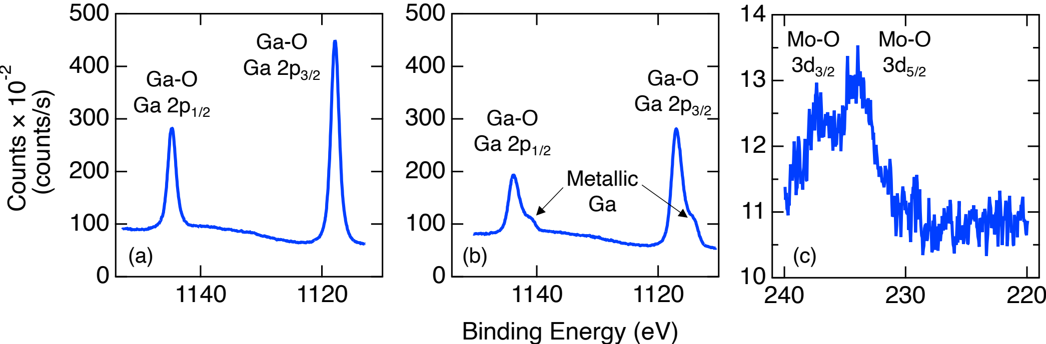

FIG. S5. X-ray photoelectron spectroscopy (XPS) data is shown for (a) the control sample, G2, (b)-(c) the Mo capped sample, M3.

After the 900°C anneal and after the wet etch to remove the mask, *ex-situ*, X-ray photoelectron spectroscopy (XPS) was performed on samples G2 (control sample), M2 (SiO_2 capped sample), M3 (Mo capped sample), and a non-annealed Ga_2O_3 sample. XPS was performed in a Scienta Omicron ESCA2SR system using monochromatic Al $K\alpha$ X-ray source (1486.7 eV) with a pass energy of 150 eV for the survey scans and a pass energy of 30 eV for the high resolution scans of core levels.

Figure S5(a) shows the data for sample G2. The Ga 2p core level region shows a Ga-O bonding environment which is expected for Ga_2O_3. The same behavior is observed for the non-annealed, reference sample (not shown). The SiO_2 capped sample, M2, was measured (not shown) after the cap was removed by wet etch. The XPS results are comparable to that of G2. No Si was observed in the Si core level regions indicating the SiO_2 cap had been fully removed. Measurements of the Mo capped sample, M3, are shown in Fig S5(b)-(c). Figure S5(b) shows the Ga 2p region where, as expected, Ga-O bonding occurred. Additionally, Ga-Ga metallic bonding was observed, as indicated by the shoulder on the peak. This was unique to the M3 sample. The Mo 3d core level region is highlighted in Fig S5(c). The Mo 3d region indicates the presence of oxidized molybdenum on the sample surface indicating that, evidently, the Mo reacted and formed MoO_x which was not removed by the wet etch. The fact that MoO_x formed lends some credence to the proposed explanation for the amorphization of the Mo capped, Ga_2O_3 film, which is that, the Mo mask underwent a reaction when annealed, formed MoO_x, which affected the thermodynamics of the α-Ga_2O_3 system, leading to the eventual amorphization of the film upon cooling. However,

this is still speculative and needs further study.

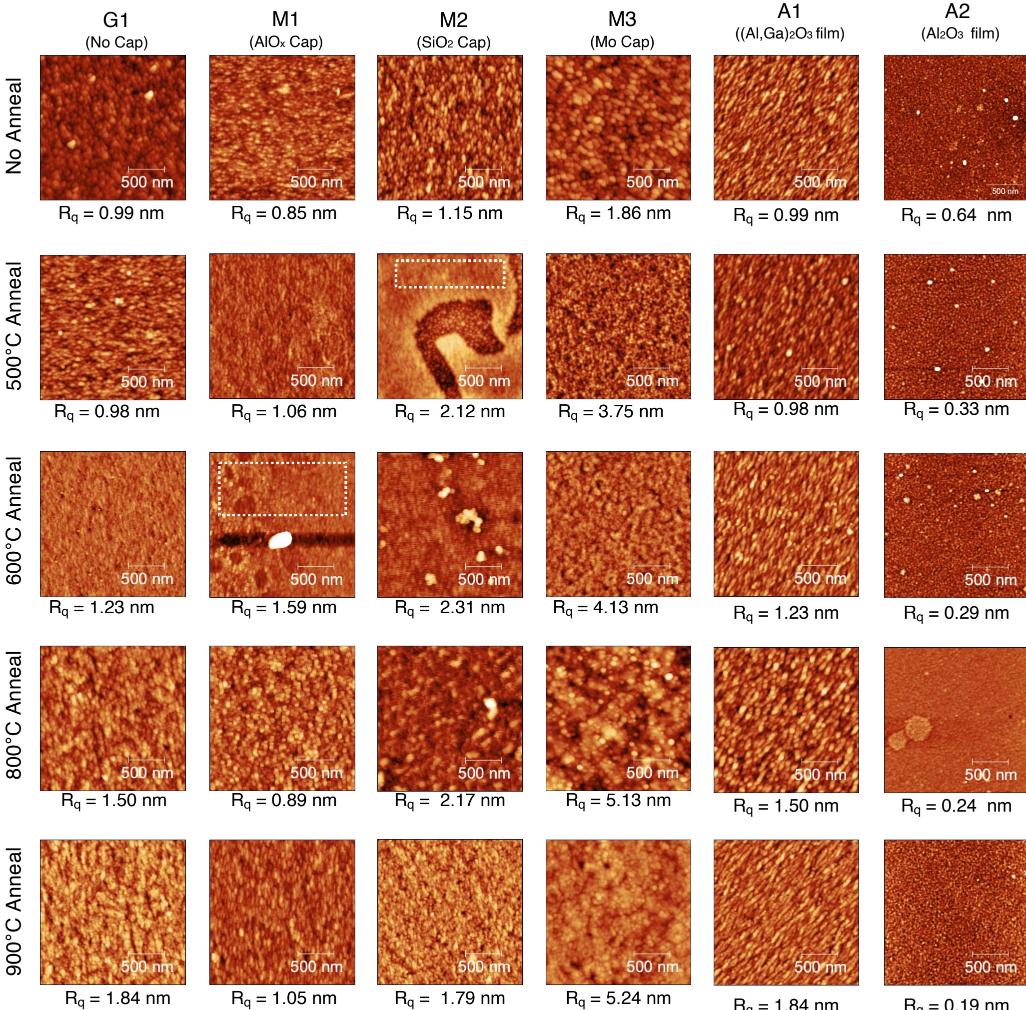

FIG. S6. The AFM images of all samples after each anneal are shown.

All AFM images for each anneal step are shown in Fig. S6. The dashed boxes for sample M1 after the 600°C anneal and sample M2 after the 500°C anneal indicate the area in which roughness was measured. The pit in sample M2 was there before annealing was started. It is also worth noting that because the MoO_x compound was not removed during the wet etch, it is not known how much, if any, of the M3 sample roughening observed with AFM was due to intrinsic roughening of the Ga_2O_3 film, intrinsic roughening of the Mo cap, or roughening of the cap due to the chemical reaction.

Figure S7 shows the extracted bandgaps for the Mo capped sample, M3, which was not shown in the main text, along with the figures from the main text for reference. The bandgap was determined

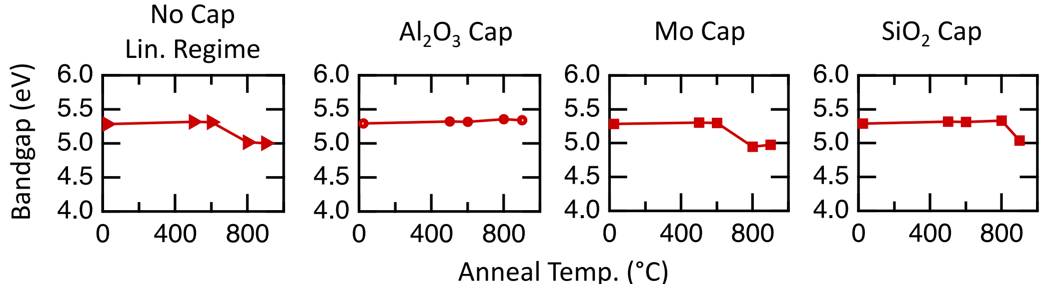

FIG. S7. The extracted bandgap values are reported for the Mo capped sample which was not shown in the main text, along with the other samples as reference

by taking the 1st derivative of the Tauc plot to find the inflection point. The x-intercept of a line drawn tangent to the inflection point was the reported bandgap value.

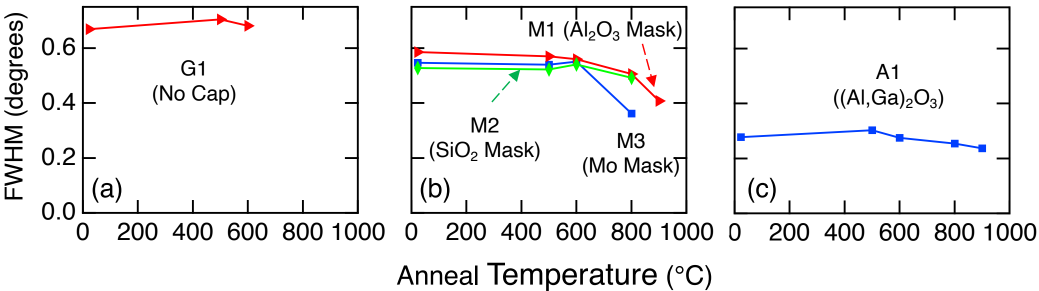

FIG. S8. The rocking curve full-width at half-max (FWHM) values are shown as a function of anneal temperature for (a) the control sample G1, (b) the masked samples, and (c) the $(Al, Ga)_2O_3$, sample A1.

In Fig. S8, the full-width at half-max (FWHM) is reported for the samples after each annealing step. The measurement is performed on the $30\bar{3}0$ diffraction peak of the α-$(Al, Ga)_2O_3$ films. If the sample converted to the β-phase or became amorphous, no value is reported. No measurement was made of sample A2, the Al_2O_3 epitaxially grown sample.

Sample M3 had a very low intensity rocking curve value after the 800°C anneal. This is due to the structural degradation as the sample became amorphous. As a result, the signal to noise ratio was reduced. Therefore, this FWHM value is not necessarily representative of the sample.